Regional Studies in Marine Science 29 (2019) 100620

Contents lists available at ScienceDirect

Regional Studies in Marine Science

journal homepage: www.elsevier.com/locate/rsma

On the role of the bay of algeciras in the exchange across the strait of Gibraltar

Jesús García Lafuente, Simone Sammartino, José C. Sánchez Garrido, Cristina Naranjo *

Physical Oceanography Group, Department of Applied Physics II, University of Málaga, Málaga, Spain

ARTICLE INFO

Article history:
Received 15 June 2018
Received in revised form 8 February 2019
Accepted 3 April 2019
Available online 27 April 2019

ABSTRACT

The role that the Algeciras Bay, a medium size embayment located in the eastern part of the Strait of Gibraltar, may have on the water exchange through the Strait and on other physical properties of the area has been numerically investigated using different configurations of a numerical model. Three domains have been considered, the present configuration with the Bay and two other configurations in which the Bay is suppressed either by filling the embayment, which produces a longer Strait, or by removing the Gibraltar Rock and isthmus, which gives rise to a shorter Strait. Only little modifications are produced in the mean properties, the shorter Strait increasing very slightly the mean exchange and diminishing the cross-section averaged salinity of the inflow. The spatial pattern of semidiurnal tidal ellipses is changed in the vicinity of the Bay, but other properties such as the minimum amplitude of semidiurnal M_2 transport that occurs off the Bay in the Strait and that could be related to the present configuration, remain unaltered. It is speculated that the main consequence of suppressing the Bay relates to the export of primary production, as it acts out as a buffer of water with residence times long enough to sustain high levels of productivity.

1. Introduction

Studies addressing the water exchange through the Strait of Gibraltar have not paid much attention to the role that the Algeciras Bay, a medium-size embayment located at the eastern part of the Strait (Fig. 1), may have on the water exchange. However, the presence inside the bay of the port of Algeciras, which holds a heavy maritime traffic of fuel and general supplies with potential risk for environmental pollution, raises issues of strategic importance which have motivated studies of the circulation and renewal mechanisms of the embayment (Periáñez, 2012; Sammartino et al., 2014, 2018; Sánchez Garrido et al., 2014; Chioua et al., 2017). All these studies address the influence of the Strait's dynamics on the circulation of the Bay, but not the opposite. This is, they do not investigate the possible influence of the Bay on the exchange flow occurring in the Strait, neither its spatial reach in case there is any.

The hydrodynamics of the Strait is complex. Many theoretical, numerical and experimental studies have been focused on the Strait of Gibraltar during the past decades (see García Lafuente et al., 2017, and references therein for a recent review). All of them emphasize the importance of tidal flows, not only by their notable amplitude that may reach 4 Sv (Sverdrup; 1 Sv $= 10^6$ m^3 s^{-1}), but also by their contribution to the long term exchange via eddy fluxes and mixing (Bryden et al., 1994; Naranjo et al., 2014). Tides prevail largely over any other external force and dominate the instantaneous exchange. The strong flow–topography interaction originates a remarkable first-mode baroclinic tide in the main sill of the Strait (Camarinal sill, see Fig. 1), which radiates away zonally in both directions with a phase speed of c $\approx$ 1 to 1.5 m s^{-1} (Armi and Farmer, 1988; Sánchez Garrido et al., 2011). The superposition of this internal tide with the barotropic tide gives rise to a marked asymmetry in the spatial pattern of semidiurnal tidal flows, with decreasing tidal transports from west to east in the Atlantic layer, and from east to west in the Mediterranean layer (Sánchez Román et al., 2012). Subinertial variability (O(10 days)) follows tides regarding the energy of flow fluctuations. It is mainly driven by the atmospheric pressure variations over the Mediterranean Sea (Candela et al., 1989; García Lafuente et al., 2002) and causes fluctuations of few tenths of Sv amplitude, which is an order of magnitude less than tidal flows. Seasonal and interannual fluctuations are also present, although they are considerably weaker than the meteorologically-induced subinertial variability (Sammartino et al., 2015). Therefore, the basic characteristic of the Strait is the long-term baroclinic exchange modulated – and greatly masked – by tidal fluctuations at shorter time-scales.

The Algeciras Bay is a natural south-southeast-facing inlet, 8–10 km wide and 10–12 km long, with a surface area of about 73 km^2 (∼6% of area of Strait) with end-points in Point Carnero to the west and Point Europa to the east (Fig. 1). The bathymetry

* Corresponding author.
E-mail address: cnaranjo@ctima.uma.es (C. Naranjo).

https://doi.org/10.1016/j.rsma.2019.100620
2352-4855/

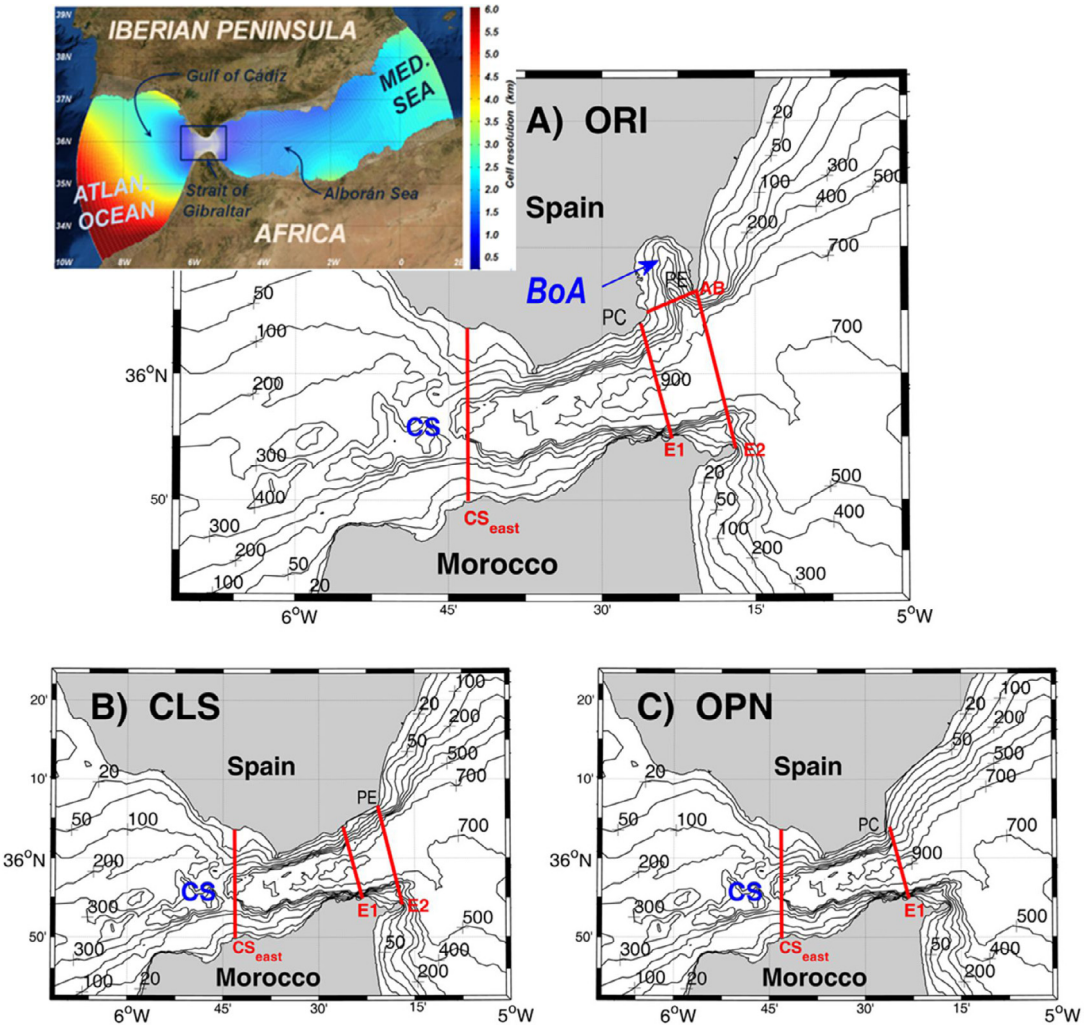

Fig. 1. Different configurations of the Strait of Gibraltar investigated in this study. Panel (A) is the present geometry (ORIginal configuration) showing the location of the Bay of Algeciras (BoA). Panel (B) represents a Strait in which the Bay has been filled with land and the bathymetry changed accordingly (CLoSed configuration). Panel (C) is the version in which the Gibraltar Rock and isthmus have been removed and, again, the bathymetry modified accordingly (OPeN configuration). Sections E1, E2, AB and CS_{east}, mentioned in the text are indicated. CS stands for Camarinal Sill, the main sill of the Strait of Gibraltar. PC and PE indicate Point Carnero and Point Europa, respectively, the ending points of the Bay of Algeciras in its present-day shape. Overlapped on the upper-left corner of panel (A) is the model domain that shows the mesh and the grid resolution. The rectangle highlights the enlarged area in panels (A) to (C) on which the modified configurations have been accomplished.

shows a central canyon that sinks steeply to a maximum depth of 450 m at the southern limit and that keeps on plunging deeper southwards. All the above mentioned processes have characteristic length-scale much greater than the Bay dimensions, reason for which we can anticipate little influence of the Bay in the exchange through the Strait. There are, however, some issues that could shed doubts on the previous assertion. For instance, the baroclinic tide has a length-scale ($\sim\lambda = cT$) of $\sim$50 km, which is comparable to the dimensions of the Bay. The amplitude of the M_2 tidal transport in the Atlantic layer at section E1 in the eastern Strait (see Fig. 1) is 0.33 Sv (García Lafuente et al., 2000), whereas it is 0.061 Sv across the southern boundary of the Bay (section AB, Fig. 1), according to Sammartino et al. (2014). It represents a 20% of the transport across section E1, a proportion that increases to the east as M_2 transport in the Atlantic layer decreases in this direction (Sánchez Román et al., 2012). Also, the dimensions of the Bay are comparable to the width of the Strait (14 km at its narrowest section).

Regarding biological processes, the Bay plays the role of a buffer for surface waters (Sammartino et al., 2014), which are easily enriched because the Earth rotation causes a northward slope of the interface that brings the nutrient-rich Mediterranean water close to the surface over its northern area (Sammartino et al., 2014). Sánchez Garrido et al. (2014) estimated a residence time of 4 days ($\sim$8 tidal cycles) for these surface waters in the Bay, a period that can be doubled or tripled if short-scale morphologic details, either man-made or natural, are considered (Sammartino et al., 2018). This time is long enough to enhance the primary production, which is eventually exported to the adjacent Alboran Sea, as suggested by Fig. 2. It provides an example on how the influence of small-scale features exceeds their own dimensions.

All the above provides reasons to address the question of whether or not the Bay influences the Strait dynamics (at least in its easternmost part), even if an analysis of the length-scales of the processes involved and of the Bay itself anticipates little variations. Numerical models offer a good chance to assess this influence as the Bay can be easily removed from the simulated domain (the way in which the exclusion has been achieved is detailed in the next section). Numerical outputs produced by different configurations can be compared and analyzed in order to address a set of questions like does the mean exchange through the Strait vary significantly under the different configurations?

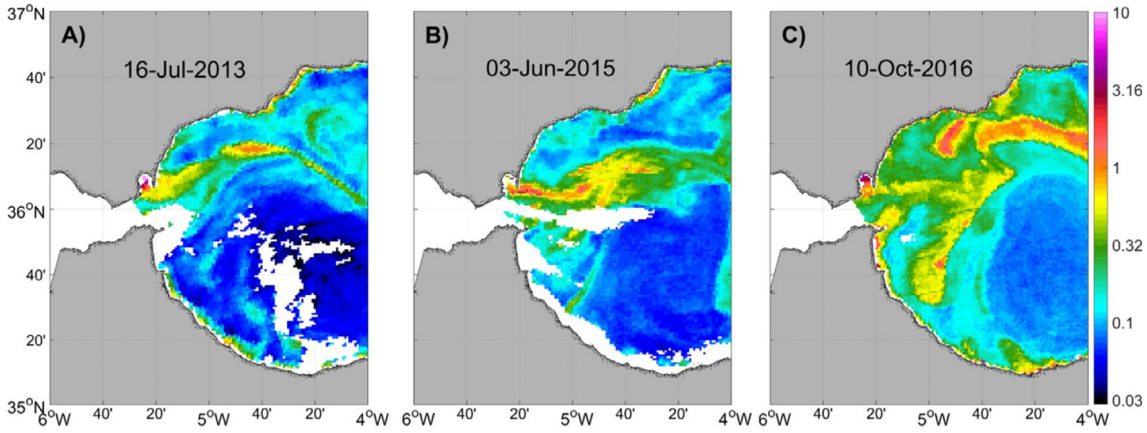

Fig. 2. Remotely sensed surface chlorophyll concentration (mg m^{-3} color scale on the right) provided by CMEMS and distributed by Copernicus (http://marine.copernicus.eu). The data are originally distributed by the Group for Satellite Oceanography (GOS-ISAC) of the Italian National Research Council, (CNR, Rome, http://www.globcolour.info/) that produces sea surface color images at spatial resolution of 1 km by merging data from the sensors MODIS-Aqua and NPP-VIIRS sensors (Volpe et al., 2012). Panels (A), (B) and (C) show three images on the dates indicated which display a chlorophyll-rich filament emanating from the Algeciras Bay, where maximum concentration is systematically found.

Are tidal transports modified and to what extent? How is the spatial structure of tidal currents affected? Are the mean hydrological properties of the inflow and outflow (salinity in our case) modified and, if so, to what extent? They are addressed in this study according to the following organization: Section 2 presents the numerical model and provides details about the altered model bathymetry. Section 3 revisits the main features of the present exchange that are prone to be modified under the alternate configurations. Section 4 addresses the above formulated questions in detail and Section 5 summarizes the conclusions.

2. The numerical model and domain configurations

The numerical model used is the Massachusetts Institute of Technology general circulation model (MITgcm) that solves the Boussinesq approximation of the Navier–Stokes equations for an incompressible fluid (Marshall et al., 1997). The model domain covers the Gulf of Cádiz (Atlantic Ocean) and Alborán (Mediterranean Sea) basins (see upper-left inset in Fig. 1). It uses a curvilinear computational grid with maximum spatial resolution in the Strait of Gibraltar (around 500 m mesh size) that decreases towards the adjacent basins to a minimum of around 5 km in the southwest part of the domain (see inset in Fig. 1). The grid is unevenly spaced in the vertical (a total of 46 cells), with cell thickness increasing from 5 m in the surface to 250 m in the deepest level. However, in area of the Strait on which the study focus (Fig. 1A) the maximum depth is ∼1000 m which corresponds to level 32, whose thickness is 98 m.

Lateral boundary forcing includes three terms. The first one is the daily 3D fields of temperature, salinity and baroclinic horizontal velocity derived from the Copernicus Marine IBI Ocean Analysis and Forecasting system (Sotillo et al., 2015). This model does not account for the subinertial flows mainly driven by changes of atmospheric pressure over the Mediterranean, which are well reproduced by the HAMSOM model integrated in the Nivmar storm surge forecast system (Álvarez Fanjul et al., 2001; García Lafuente et al., 2002). The meteorologically-induced barotropic velocity is the second contribution. Finally, tides are introduced by generating barotropic tidal currents at the boundaries using the harmonic constants derived by the Mog2D model (Carrère and Lyard, 2003). Additionally to the former lateral forcing, the model includes heat and mass fluxes across the sea surface imported from the HIRLAM atmospheric model of the Spanish Meteorological Agency forecast service (Cats and Wolters, 1996; Navascues et al., 2013) which accounts for seasonal and interannual variability. Initial conditions are also extracted from Sotillo et al. (2015).

This numerical model has been previously used in several oceanographic studies of this region (Sánchez Garrido et al., 2013, 2014; Sammartino et al., 2014; we refer to the latter for a detailed description of the model setup and validation). Since 2012 the model is routinely run within an operational oceanography system implemented in the Strait of Gibraltar by the Spanish Port Authority (http://portus.puertos.es; see also Sánchez Garrido et al., 2013).

Because of the large prevalence of tides in the flow variability and with the aim of keeping the essential, in this study the model has been only forced by the baroclinic field imported from MyOcean-MED and the barotropic tide. Whatever the influence the Algeciras Bay may have in the global hydrodynamics of the Strait, the expectedly most influenced frequency band is the tidal band, which becomes the main focus of the present study. Therefore, the focus of the study is whether or not hypothetical morphological changes in the Strait affect the presently observed tide and mean exchange via eddy-fluxes. Three domain configurations with the same open boundaries have been investigated, the differences lying in the Strait geometry over the area around the Bay of Algeciras. The first one (the reference configuration referred to as ORI henceforth) is the present coastline (Fig. 1A). The second one is built by filling the whole embayment until section AB in Fig. 1A, which gives rise to a strait longer than nowadays (CLS configuration, Fig. 1B). The implied isobaths have been consequently modified to smoothly merge with the unmodified portions of the same isobaths, as shown in Fig. 1B. Last configuration removes the Gibraltar rock and isthmus, featuring a Strait shorter than the present one (OPN configuration, Fig. 1C). Implied isobaths have been reshaped accordingly.

The prescribed boundary conditions are the same in all three cases. After a spin-up period of one month, during which the model solution evolved from the initial conditions to a steady periodic solution of the exchange, we completed additional 32 days of simulation (March 29, 2013–April 30, 2013), storing hourly outputs of the 3-D fields of salinity, temperature and velocity as well as the 2-D field of sea level height. These series are suitable to achieve our objective since they are long enough for resolving the main semidiurnal and diurnal tidal constituents and they form the basis of our analysis.

3. A review of features of the exchange addressed in this work

3.1. Mean exchange and the interface salinity

Fig. 3A shows the mean inflow computed from the model (the mean outflow is not shown because, in the absence of meteorological forcing, it is the specular image of the inflow in order to produce a null net flow). The mean inflow/outflow computation is not straightforward because tidal currents prevail in the instantaneous velocity field. Any layer (Mediterranean, Atlantic) can move in either direction due to tidally-induced current reversals and, therefore, the flow direction (velocity sign) is not a suitable criterion for layer identification. Following García Lafuente et al. (2000) (see also Naranjo et al., 2014, for details), a material surface (isohaline) is used as interface, which is a more realistic criterion. The selected isohaline is the one that maximizes the time-averaged inflow and outflow during a period much longer than the semidiurnal time-scale. The referred isohaline changes from one cross-section to another due to water entrainment from one layer into the other. Fig. 3B shows the well-known result that the salinity of the interface increases from west to east. Fig. 3A illustrates the spatial variations of the mean inflow or Atlantic layer transport that shows a local minimum nearby the sill of Camarinal (in CS_{east} section, see Fig. 1), another well-known pattern of the exchange (see Sannino et al., 2004, for instance). Eastwards (westwards) from this site, the Atlantic transport increases due to the entrainment (detrainment) of water from (to) the Mediterranean layer. Fig. 3C shows the mean depth of S = 37.0 to illustrate the shoaling of isohalines towards the east. Dashed lines are 1std apart from the mean depth and give hints on the size of internal oscillations associated with tides. It reaches a maximum value around the main sill.

3.2. Tidal transport

Fig. 4 illustrates other known characteristics of tidal transports in the Strait that are of concern in this study. They have been already discussed in the literature (Sánchez Román et al., 2012). Harmonic constants of transports have been computed using standard packages of harmonic analysis (Pawlowicz et al., 2002) applied to the time series obtained in the way explained above. Fig. 4A shows how the amplitude of M_2 transport in the Atlantic layer (blue line) decreases noticeably from west to east, whereas the Mediterranean layer (red line) behaves oppositely. This opposite behavior is consequence of the internal hydraulic control over the sill of Camarinal that limits the size of the exchanged flows at tidal time-scale too (Sánchez Román et al., 2012). However, the net tidal transport (green line) has no spatial structure except for the slight and smooth east-to-west decrease of the amplitude necessary to account for the vertical tide. Its phase is constant at around 130° in quadrature with the phase of sea level, in agreement with the standing wave nature of the tide in the Strait (Defant, 1961; García Lafuente et al., 1990; Candela et al., 1990). This pattern does not apply to the layer transports. In particular, the Atlantic layer phase shows a steady increase eastwards of Camarinal sill until a short distance after section E1, where it suddenly drops. The increase implies wave progression with a wave celerity of c_v = 3.5–4 m s^{-1}, as suggested by the phase slope. The fast drop eastwards of section E1 coincides with a minimum of amplitude and, interestingly, they are found between sections E1 and E2, off of Algeciras Bay (see Fig. 1). We will return to this issue. The M_2 pattern is applicable to other semidiurnal constituents (not shown). Diurnal K_1 tidal transports (Fig. 4C and D) share some of the semidiurnal characteristics such as the west-to-east (east-to-west) amplitude increase in the Atlantic (Mediterranean) layer, or the eastward phase increase in the Atlantic layer. But they neither show any local amplitude minimum nor a sharp phase variation nearby Algeciras Bay.

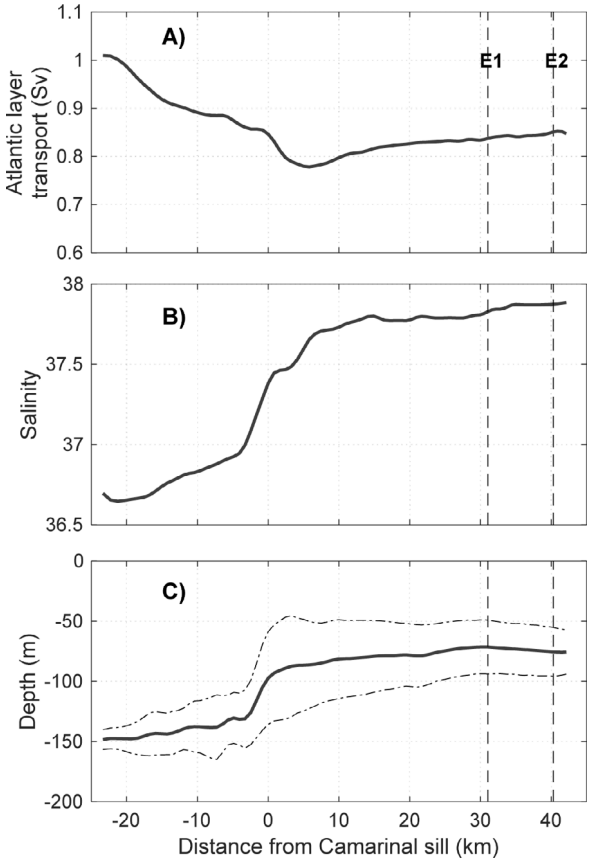

Fig. 3. (A) Time-averaged Atlantic layer transport (inflow) in Sv (1 Sv = 10^6 m^3 s^{-1}), which changes in the along-strait direction, showing a minimum near Camarinal sill to the east (in CSeast section, see Fig. 1 for location). (B) Salinity that maximizes the time-averaged flow, which has been selected as the interface in order to compute flows (see text). (C) Mean depth of the 37.0 isohaline along the mid-axis of the Strait, which shows the isopycnal shoaling from west to east. Dash-dotted lines are ±1 std distance of the mean depth to illustrate the large tidally-induced vertical oscillations of internal surfaces. Sections E1 and E2 are indicated (see Fig. 1A for location).

3.3. Internal tide in the eastern half of the Strait

Internal oscillations of isohalines are the best tracer of the remarkable internal tide regularly generated in the main sill of the Strait. Black line in Fig. 4A shows the M_2 amplitude of the internal oscillation, which peaks nearby Camarinal sill and then decreases towards both sides (see also Table 1). At the eastern part, between sections E1 and E2 the amplitude diminishes to 15 m, depicting a local minimum. The phase (Fig. 4B, black line) increases steadily with constant slope from the sill to the east. It mimics the behavior of the phase of the transport (blue line) with two worth-mentioning differences: First, the sudden drop in transport phase is not found in the oscillation, which maintains the positive slope all the way through and, second, the slope of the internal oscillation is steeper than that of the transport, indicating slower wave celerity for the oscillation wave c_h. A straightforward computations gives c_h = 2.3–2.4 m s^{-1}, which agrees with reported values from observations (Farmer and Armi, 1988; Sánchez Garrido et al., 2008) and previous modeling works (Sánchez Garrido et al., 2011). Actually it is the expected value for a first-mode baroclinic wave in a stratified environment with the characteristics of the Strait (c ≈ 1.5 m s^{-1}) advected by a background flow of U ≈ 1 m s^{-1}. An explanation for the c_v and c_h mismatch is that internal interface oscillation is a

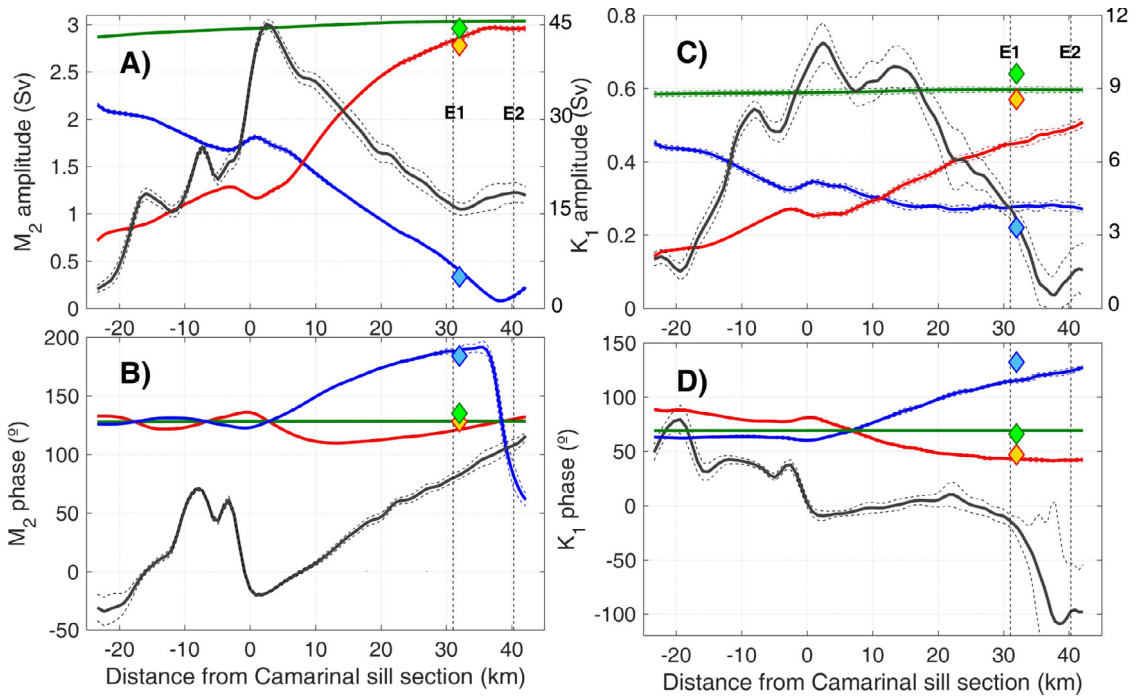

Fig. 4. Harmonic constants for M_2 and K_1 constituents according to the following code: Blue, red and green lines are for Atlantic, Mediterranean and total transport, respectively; black line is for vertical oscillation of isohaline S = 37.0 along a central longitudinal section following the axis of the Strait, which has been taken as representative of the internal surfaces. All plots are function of the along-strait distance measured from Camarinal sill section (km 0). Panel (A) is for M_2 amplitude (transport in Sv, left scale; isohaline oscillation in m, right scale). Panel (B) is for M_2 phases. Panels (C) and (D) are the same as panels (A) and (C) except for K_1 constituent. Dashed lines in all plots indicate the error of the estimated harmonic constants. Filled diamonds correspond to the values of M_2 and K_1 transports reported in García Lafuente et al. (2000) at a section close to E1, using the same color code as for the lines . (For interpretation of the references to color in this figure legend, the reader is referred to the web version of this article.)

purely baroclinic motion whereas the transport computation involves tidal currents which have an extra barotropic contribution added to the baroclinic motion (García Lafuente et al., 2000). The amplitude of diurnal oscillations, as represented by K_1, shows maximum values nearby the sill, resembling M_2 (black lines in Fig. 4C and D) and, again, a local minimum between sections E1 and E2 that approaches zero in this case, indicating little baroclinic motion. The coincidental and somewhat erratic behavior of the phase (dashed black lines in Fig. 4D) would be related to the smallness of the amplitude.

3.4. Tidal currents

Fig. 5 shows the tidal ellipses for M_2 and K_1 in the surroundings of Algeciras Bay at two levels in the Atlantic (1 m) and Mediterranean (250 m) layers. At 1 m depth and at a short distance west of section E2, M_2 ellipses almost vanishes (Fig. 5A). This pattern, which extends downward a few tens of meters in the Atlantic layer, agrees with the observations reported in Soto-Navarro et al. (2016), and would explain the amplitude minimum of M_2 transport visible in Fig. 4A. Ellipses phase changes on each side of section E2 (see enlarged ellipses at the bottom of Fig. 5A), in agreement with the quick phase variation observed in Fig. 4B. The notable penetration of the semidiurnal tide into Algeciras Bay, already reported in Sammartino et al. (2014), is clearly depicted by the meridional orientation of the tidal ellipses. In the Mediterranean layer (250 m depth, Fig. 5B) the ellipses are quite similar all over the area and larger than at the surface (consider the ellipses at the bottom of Fig. 5B, enlarged by the same factor as in Fig. 5A, for comparison). Their phases are similar to those of surface ellipses west of section E1 and they do not undergo the above mentioned phase change of the surface ellipses nearby and east of section E2. In the Algeciras Bay, the ellipses eccentricity is almost 1 (straight lines) and are meridionally oriented along the submarine canyon of the Bay. Notice that this pattern is necessary for compensating the surface penetration of the tide.

Diurnal constituents, represented by K_1, show little spatial variation. The horizontal pattern is very regular (Fig. 5C and 5) and, in contrast to what happens with the semidiurnal M_2, the amplitude decreases monotonically as we proceed downwards. Diurnal energy hardly penetrates into Algeciras Bay, as the ellipses remain orientated in the zonal direction.

3.5. The averaged inflow salinity

The inflow density has implications in the overall thermohaline circulation of the Mediterranean Sea, particularly regarding the processes of deep water formation, as discussed in Naranjo et al. (2014) or Sannino et al. (2015). Since most of the density contrast between inflow and outflow waters is due to salinity differences, we have considered the cross-section averaged salinity as the relevant variable to distinguish both water masses. Table 1 shows that the inflow salinity increases from west (section CS_{east}) to east (section E2), while the outflow salinity behaves oppositely. It is the expected pattern for a strongly sheared flow with entrainment-driven vertical exchange of water between layers, as discussed in García Lafuente et al. (2013).

4. The modified versus the original domains

The outputs of the numerical model for the three studied configurations are now compared in order to investigate and assess possible changes regarding the topics described in the previous Section. It is important to remark that the numerical runs have been performed with identical boundary conditions, the only change being the domain differences in morphology and bathymetry.

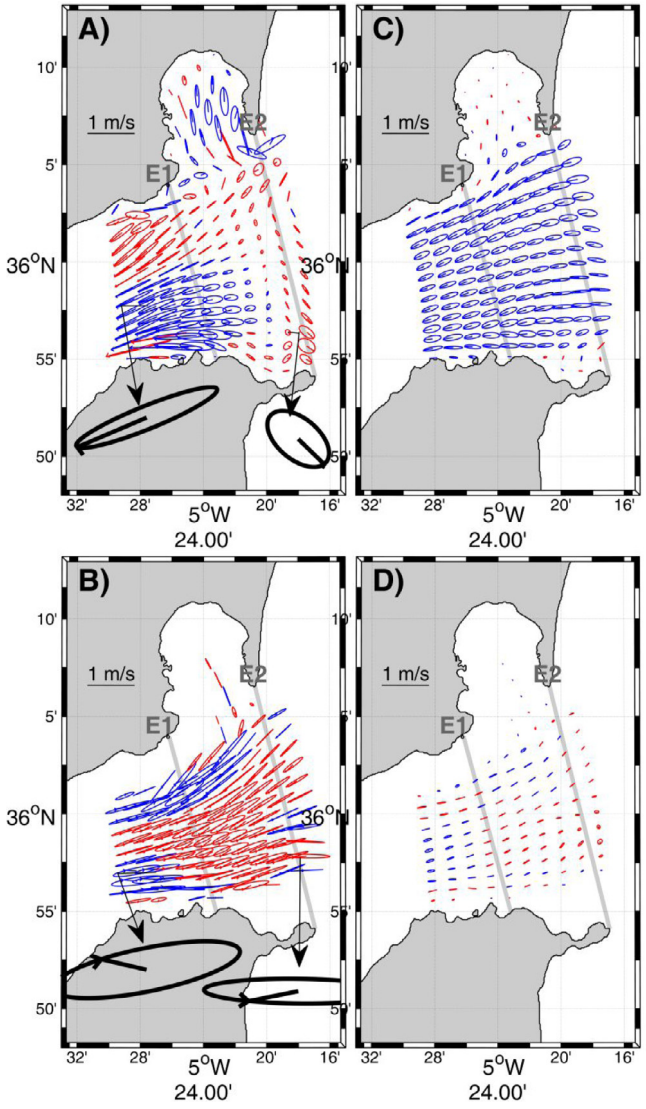

Fig. 5. (A) Tidal ellipses for M_2 constituent at the surface. Blue and red colors mean clockwise and anticlockwise rotation, respectively. The small straight lines inside the ellipses indicate the phase, which are better seen in the enlarged black ellipses at the bottom of the panel. The velocity scale in the upper-left part of the panel only stands for the colored ellipses, not for the black ones. Sections E1 and E2 have been indicated. (B) Same as (A) for currents at 250 m depth. Panels (C) and (D) are the same as (A) and (B) except for K_1. Only ellipses have been drawn in one out of every four grid points in the zonal direction and one out of every three in the meridional direction for clarity reasons. (For interpretation of the references to color in this figure legend, the reader is referred to the web version of this article.)

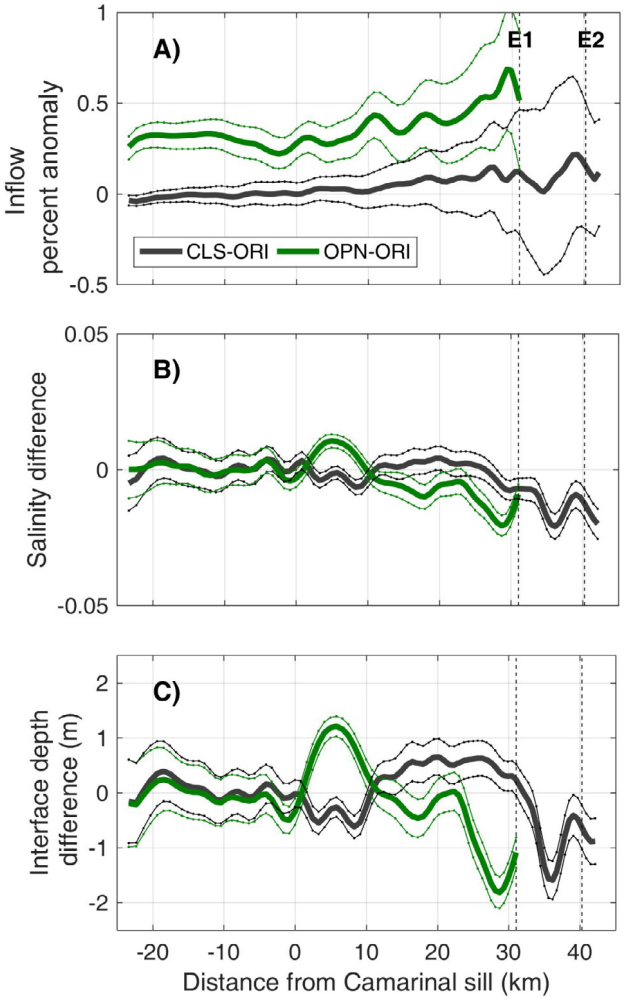

Fig. 6. (A) Percent variation of the time-averaged inflow computed as the values obtained in CLS or OPN configurations minus that one in ORI configuration, normalized by the latter (see Eq. (1) in the text for details and the legend for the color code). (B) Salinity difference between the interfaces computed in CLS/OPN and ORI configurations (CLS–ORI and OPN–ORI, see color code in legend). (C) Same as (B) except for interface depth. This depth has been taken as a positive number, so that negative values of the difference imply a deeper interface in ORI configuration. Sections E1 and E2 are indicated. Green lines end in section E1, which is the easternmost section of the Strait for OPN configuration (see Fig. 1C). Dashed lines indicate the confidence interval of the estimations. (For interpretation of the references to color in this figure legend, the reader is referred to the web version of this article.)

4.1. Mean exchange and interface; internal tide

Fig. 6A shows the percentage of the mean inflow transport difference with regard to the original configuration (see Fig. 1 for the geometry of the domains) computed according to

$$Percent = \frac{Mod.Config - ORI.Config}{ORI.Config} \times 100 \qquad (1)$$

where *Mod.Config* is either CLS or OPN configurations. Differences are below 0.2% and are not significant in the CLS domain and a little larger in the case of OPN, although less than 1% everywhere. Even if small, the regular positive difference in the OPN case, which is significant, suggests that this configuration propitiates a slightly greater exchange, a conclusion that could not be extended to the CLS case. Fig. 6B shows the salinity difference of the isohalines that maximize the exchange, i.e., of the interface. East of Camarinal sill, OPN–ORI oscillates giving differences significantly different from zero just east of the sill, whereas CLS–ORI is not different from zero until the region between sections E1 and E2 off the Bay of Algeciras. Since salinity increases with depth, negative values of the difference imply deeper interface of the second term, which is ORI in both cases. The depth differences (Fig. 6C; notice the resemblance with Fig. 6B) are small everywhere and reach the greatest values between sections E1 and E2 in CLS, and nearby section E1 in OPN, the ORI interface being deeper in both situations. In the first case, the presence of the Bay in ORI configuration that broadens the cross-area of the inflow and diminishes the flow speed could make the interface sink a little for continuity. In the OPN case, the behavior would be related to the fact that section E1 is the eastern exit in this configuration (Fig. 1C).

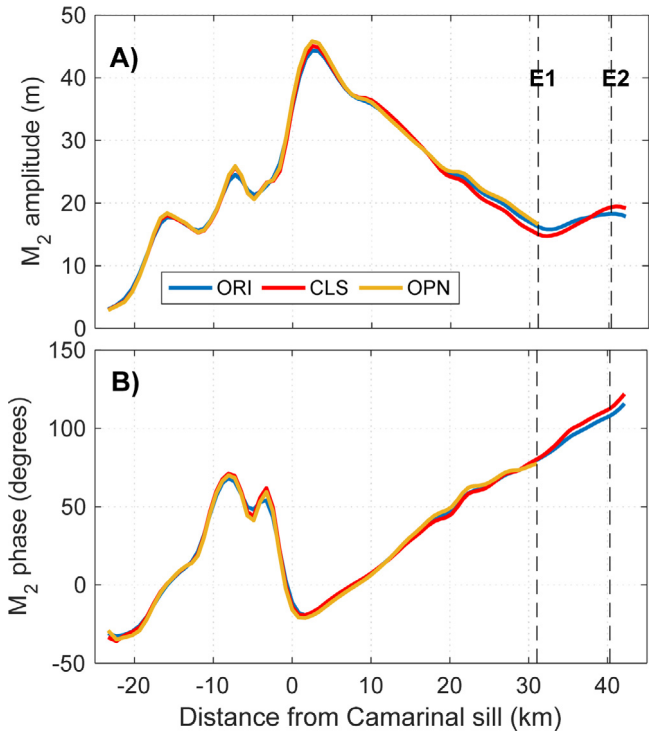

Fig. 7. (A) M_2 amplitude (m) of the isohaline S = 37.0 oscillations along a central longitudinal section that follows the axis of the Strait for the three configurations (see legend). (B) Same as (A) but for M_2 phases. Sections E1 and E2 are indicated. Deep yellow lines, which correspond with OPN, end in section E1, the easternmost section of the Strait in this configuration. (For interpretation of the references to color in this figure legend, the reader is referred to the web version of this article.)

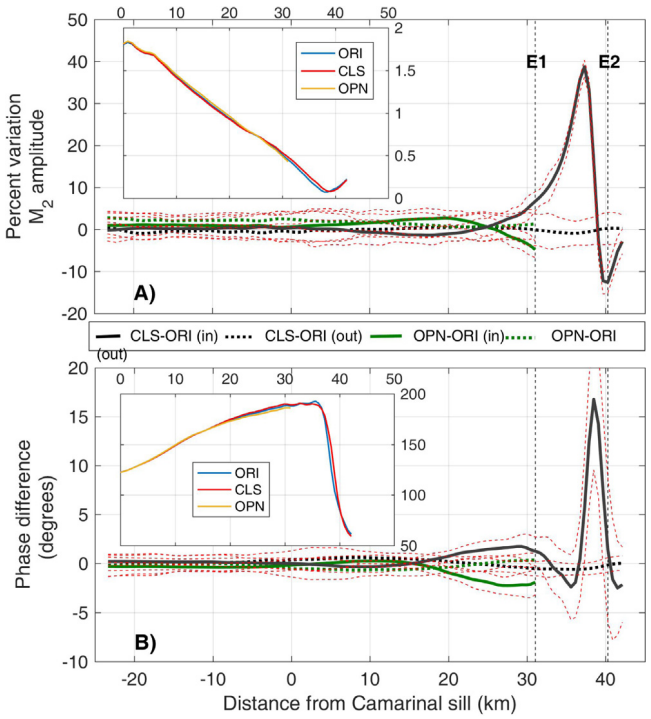

Fig. 8. (A) Percent of variation of M_2 transport amplitude computed as the values obtained in CLS/OPN configurations minus that one in ORI configuration, normalized by the latter (see Eq. (1) in the text). Black (green) lines are for the CLS (OPN) versus ORI comparison, and solid (dashed) lines are for the Atlantic (Mediterranean) layer transport (see the legend in between both panels). The inset in the upper left portion shows the M_2 transport amplitudes (Sv, right scale) for the three configuration in the east-of-Camarinal sill portion of the Strait (x > 0 km, top scale) according to the legend within the inset. (B) Same as (A) except for the phase difference (in degrees). The inset shows the actual values of phase (degrees, right scale) for the three configurations in the x > 0 km portion of the Strait. Red dashed lines indicate the confidence intervals. (For interpretation of the references to color in this figure legend, the reader is referred to the web version of this article.)

Internal tide, as revealed by internal oscillations (Fig. 7), is quite alike in all configurations. Actually, there are no changes between ORI and OPN configurations. Only unimportant differences in amplitude between CLS and ORI are observed east of km 20, with CLS amplitude being 0.5–1 m smaller around section E1 to become larger by ∼0.5 m in section E2 (Fig. 7A). Phases are even more alike (Fig. 7B), although the slope in the CLS configuration is slightly steeper between sections E1 and E2 off the Algeciras Bay, implying a slowing down of the wave celerity in this area. From curves in Fig. 7B, it is easy to estimate $c_{hORI} = 2.4$ m s^{-1}, which matches the celerity estimated in Section 3.3, whereas $c_{hCLS} = 2.1$ m s^{-1}. The diminution agrees with the fact that the interface is shallower in CLS, as shown in Fig. 6C (the closer is the pycnocline to mid-depth, the faster internal waves propagate), and also that CLS features a longer Strait, which allows an enhanced friction with regards to ORI configuration.

4.2. Tidal transport and tidal currents

Fig. 8 summarizes the results of the harmonic analysis of transports carried out. More details on the harmonic constants for M_2 and K_1 at key sections of the Strait are presented in Table 2.

The percentage of amplitude differences between M_2 tidal transports computed according to Eq. (1) are shown in Fig. 8A for the Atlantic and Mediterranean layers. In the Mediterranean layer the transport remains essentially unchanged in the CLS configuration and increases very slightly (∼2%) in the OPN case, although still remains non-significant. In the Atlantic layer the amplitude does not change until a few km west of section E1, and it does off the Bay of Algeciras between sections E1 and E2 in the CLS case. Something similar can be said about the phase (Fig. 8B). This noticeable variation, however, is somewhat misleading because the large increase in Fig. 8A takes place where the ORI M_2 amplitude, which is in the denominator of Eq. (1), reaches a minimum. Moreover, a closer inspection of amplitude and phase (insets in Fig. 8A and B) reveals great similitude between CLS and ORI configurations, the differences in percentage arising from the fact that CLS curves are slightly displaced to the east with regards to ORI curves, which would be probably related to the different celerity, $c_{h,ORI}$ and $c_{h,CLS}$, of the internal tide between sections E1 and E2 mentioned above. This displacement causes the large departures from zero off of Algeciras Bay seen in Fig. 8A and B. More relevant is the great similitude of the curves within the insets, which rejects any possibility that the minimum of amplitude between sections E1 and E2 commented in Section 3.2 was due to the presence of the Bay of Algeciras. Its origin must be rather ascribed to the superposition of the baroclinic tide generated by the interaction of the barotropic tide with the sharp topography of Camarinal sill and the barotropic tide itself, as suggested by García Lafuente et al. (2000), and not to the widening of the Strait due to the presence of the Bay. The results for other semidiurnal constituents are much the same as for M_2. Regarding diurnal species, amplitudes hardly change in the vicinity of the Bay and only the OPN configuration gives small changes of about 3%–4% in a short area between km 15 and 25 for the K_1 constituent in the Atlantic layer. Phases change even less, differing less than 2 degrees everywhere (plots not shown).

Table 1
Different parameters/variables of the exchange at the three sections indicated in the first column (see Fig. 1) and under the three configurations investigated (second column). The distance of the sections to the origin established at Camarinal is also indicated between brackets. Third column gives the mean inflow, in Sv (10^6 m^3s^{-1}), fourth column is the isohaline that maximizes the exchange, taken as interface in flow computations (see text), fifth and sixth columns are the cross-section averaged salinity of the inflow and outflow, respectively. The last two columns are the harmonic constants of internal oscillations of the main semidiurnal (M_2) constituent, as represented by $S = 37.0$, with the amplitude given in m and phase in degrees referred to Greenwich meridian. Section E2 in the OPN configuration is meaningless in our analysis and no values are provided. Highlighted in bold is the salinity of the inflow as it leaves the Strait and enters the Alboran Sea for each configuration.

Section	Config.	$\overline{Q_{in}}$ (Sv)	$S_{interface}$	$\overline{S_{in}}$	$\overline{S_{out}}$	$M_{2,37.0}$ A (m)	$M_{2,37.0}$ ϕ (degr)
CS_{east} (KP 5.8)	ORI	0.7759	37.685	36.684	38.391	39.7 ± 1.2	353.3 ± 1.6
	CLS	0.7760	37.685	36.684	38.392	39.8 ± 1.3	354.3 ± 1.8
	OPN	0.7783	37.690	36.689	38.388	40.1 ± 1.2	352.0 ± 1.9
E1 (KP 29.9)	ORI	0.8320	37.805	36.922	38.436	17.1 ± 1.2	76.5 ± 4.0
	CLS	0.8330	37.795	36.910	38.435	15.8 ± 1.3	77.3 ± 4.6
	OPN	0.8388	37.785	**36.945**	38.431	17.6 ± 1.3	75.5 ± 3.9
E2 (KP 40.3)	ORI	0.8509	37.870	**36.988**	38.444	18.4 ± 1.6	109.5 ± 4.7
	CLS	0.8524	37.860	**36.968**	38.444	19.6 ± 1.7	114.5 ± 4.5
	OPN	–	–	–	–	–	–

Table 2
Harmonic constants of the main semidiurnal (M_2) and diurnal (K_1) constituents for the inflow, outflow and total flow (subscripts "in", "out", and "tot", respectively) at the same three sections as in Table 1 and for the three investigated configurations. Amplitudes are given in Sv (10^6 m^3 s^{-1}) and phases in degrees referred to Greenwich meridian. Section E2 in the OPN configuration is meaningless in our analysis and no values are provided.

Section	Config.	$M_{2,in}$ A (Sv) ϕ (deg.)	$M_{2,out}$ A (Sv) ϕ (deg.)	$M_{2,tot}$ A (Sv) ϕ (deg.)	$K_{1,in}$ A (Sv) ϕ (deg.)	$K_{1,out}$ A (Sv) ϕ (deg.)	$K_{1,tot}$ A (Sv) ϕ (deg.)
CS_{east} (KP 5.8)	ORI	1.674 ± 0.026 135.7 ± 1.0	1.333 ± 0.020 118.7 ± 1.0	2.974 ± 0.011 128.2 ± 0.5	0.335 ± 0.010 132.5 ± 2.0	0.255 ± 0.007 136.5 ± 2.0	0.590 ± 0.008 134.1 ± 1.0
	CLS	1.675 ± 0.026 135.4 ± 1.0	1.328 ± 0.017 119.2 ± 1.0	2.973 ± 0.010 128.2 ± 0.5	0.333 ± 0.008 131.9 ± 1.5	0.257 ± 0.007 136.8 ± 1.5	0.590 ± 0.007 134.0 ± 1.0
	OPN	1.690 ± 0.024 135.8 ± 1.0	1.361 ± 0.018 118.0 ± 1.0	3.015 ± 0.013 127.9 ± 0.5	0.333 ± 0.010 133.8 ± 1.5	0.256 ± 0.007 135.4 ± 2.0	0.589 ± 0.008 134.5 ± 1.5
E1 (KP 29.9)	ORI	0.514 ± 0.019 188.2 ± 2.5	2.808 ± 0.027 119.2 ± 1.0	3.030 ± 0.012 128.3 ± 0.5	0.272 ± 0.011 178.8 ± 2.5	0.446 ± 0.006 108.8 ± 1.0	0.597 ± 0.007 134.2 ± 1.0
	CLS	0.538 ± 0.022 189.9 ± 2.5	2.812 ± 0.033 118.7 ± 1.0	3.029 ± 0.016 128.4 ± 0.5	0.270 ± 0.010 179.8 ± 2.5	0.451 ± 0.007 108.7 ± 1.0	0.596 ± 0.007 134.1 ± 1.0
	OPN	0.497 ± 0.015 186.0 ± 2.0	2.839 ± 0.027 119.5 ± 0.5	3.071 ± 0.013 128.0 ± 0.5	0.275 ± 0.010 176.8 ± 2.5	0.433 ± 0.006 109.3 ± 1.0	0.595 ± 0.008 134.6 ± 1.0
E2 (KP 40.3)	ORI	0.123 ± 0.020 80.3 ± 10.3	2.956 ± 0.031 130.1 ± 1.0	3.037 ± 0.012 128.3 ± 0.5	0.278 ± 0.014 189.0 ± 3.0	0.493 ± 0.013 106.6 ± 2.0	0.596 ± 0.007 134.1 ± 1.0
	CLS	0.108 ± 0.022 80.5 ± 11.5	2.963 ± 0.025 130.0 ± 1.0	3.034 ± 0.012 128.4 ± 0.5	0.277 ± 0.13 189.5 ± 3.0	0.494 ± 0.012 106.5 ± 2.0	0.595 ± 0.007 134 ± 1.0
	OPN	– –	– –		– –	– –	– –

Maps of tidal ellipses at two different levels for M_2 and K_1 constituents are presented in Figs. 9 and 10, respectively. Regarding M_2, the pattern in all configurations is almost identical west of section E1, away from the Algeciras Bay. The change of phase of tidal ellipses between sections E1 and E2 highlighted in Fig. 5A is also reproduced in OPN and CLS configurations. Significant differences can be detected in the vicinity of Algeciras Bay, which are better seen in Fig. 11, which shows the residual tidal variability between the modified and original configurations (see Figure caption). The differences reach the Mediterranean layer and are greater for the OPN configuration. Thus, the Gibraltar rock and isthmus are relatively influential on the semidiurnal currents, which have been showed to be important in the Spanish continental slope near the Strait of Gibraltar (García Lafuente et al., 1999). Regarding K_1, the three configurations show the same pattern for all intents and purposes (Fig. 10), which is further confirmed by the almost null residual tidal variability shown in panels (E) to (H) of Fig. 11. The reason must be found in the spatial pattern of K_1 in the ORI configuration, which suggests that diurnal tidal energy does not enter into Algeciras Bay (Fig. 5C or Fig. 10A; see also Sammartino et al., 2014). Therefore, the Bay has little influence on the shape of the tidal ellipses of this species outside of the embayment.

4.3. Inflow salinity

Table 1 gives the cross-section averaged values of salinity for the inflow and outflow. In section CS_{east} (see Fig. 1 for location), away from Algeciras Bay area, the averaged salinities are the same within ±0.005 units in all configurations. At section E1, the minimum salinity for the inflow is found in the CLS domain (0.012 units smaller than in ORI), and the maximum in the OPN one (0.023 units greater). The salinity of the outflow remains the same within the ±0.005 units interval. The same difference between ORI and CLS for the inflow persists at section E2 (0.020 units now), whereas the salinity of the outflow is identical in both configurations. Notice that section E2 is outside the Strait in the OPN configuration and, therefore, no values are provided.

The salinity with which the inflow enters the Alborán Sea (and, hence, the Mediterranean) is highlighted in bold for the three domains. The saltiest inflow happens in ORI configuration and the freshest one in OPN. The latter circumstance stems from the fact that section E1 is the gateway of the inflow into the

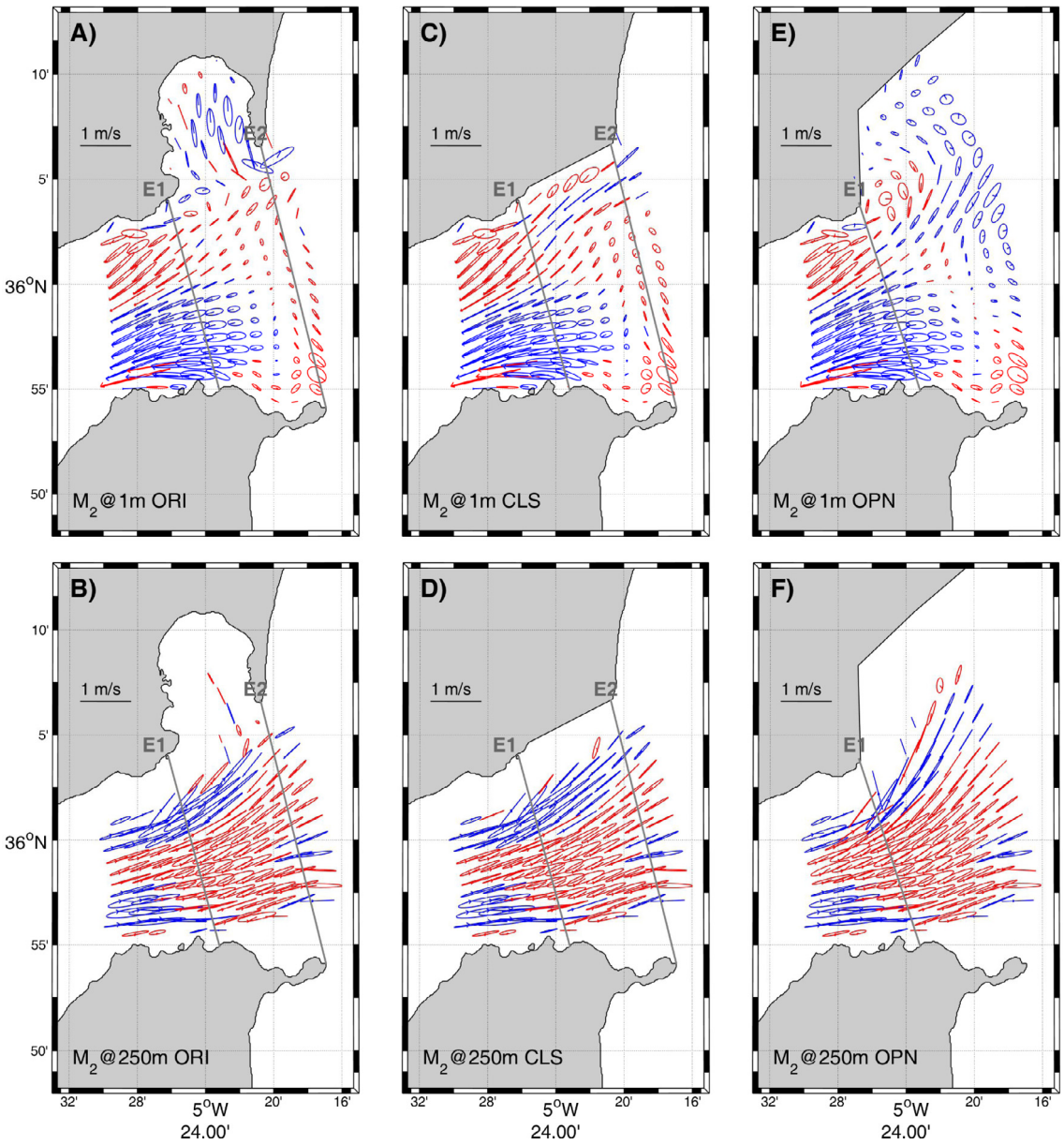

Fig. 9. (A) M_2 tidal ellipses at the surface for the ORI configuration. It is the same as Fig. 5A (except for the enlarged ellipses), and has been pointedly included here for easy comparison with the two other configurations. (B) M_2 tidal ellipses at 250 m depth for the ORI configuration (coincides with Fig. 5B). (C) and (D) Same as (A) and (B) except for CLS configuration. (E) and (F) Same as (A) and (B) except for OPN configuration. Blue (red) color indicate clockwise (anticlockwise) rotation. Sections E1 and E2 have been plotted. The results are displayed for the area around the Bay of Algeciras, where differences are expected to occur. (For interpretation of the references to color in this figure legend, the reader is referred to the web version of this article.)

Mediterranean Sea in the case of OPN configuration, whereas the entrance is section E2 for the two other configurations. Actually, OPN gives the saltiest inflow at section E1; however, the inflow goes on undergoing mixing until section E2 before leaving definitely the Strait in ORI and CLS configurations, which increases their salinities above the one of OPN configuration at section E1.

5. Discussion and conclusions

The alternative configurations of the Strait of Gibraltar generated to investigate the role of the Algeciras Bay in the tidal hydrodynamics of the Strait have shown to result in little variations with regards to the actual configuration. This result, already anticipated in the Introduction, implicitly agrees with the fact that low resolution numerical models where the Bay is very poorly represented or is even inexistent are indeed able to reproduce the main features of the exchange and the internal hydraulics of the Strait with reasonable or good accuracy (i.e., Wang, 1989; Sannino et al., 2004; Peliz et al., 2013). Minimum changes observed in the artificial configurations, most of which occurring in the neighborhood of the Bay, are summarized next.

The feature of M_2 tidal transport consisting in the marked minimum of amplitude coincidental with a sharp change of phase off of Algeciras Bay (Fig. 4, see Section 3.2), which could have been related to the widening of the Strait between sections E1 and E2 in the present configuration, is still present in the two modified domains, which rejects any possible influence of the Bay in this peculiar pattern. The minimum would be the result of the superposition of the eastward propagating baroclinic tide generated in Camarinal sill and the standing-wave barotropic tide that characterizes the overall oscillation in the Strait (García Lafuente et al., 1990), in which case the altered domains are unable to modify this rather large-scale interaction.

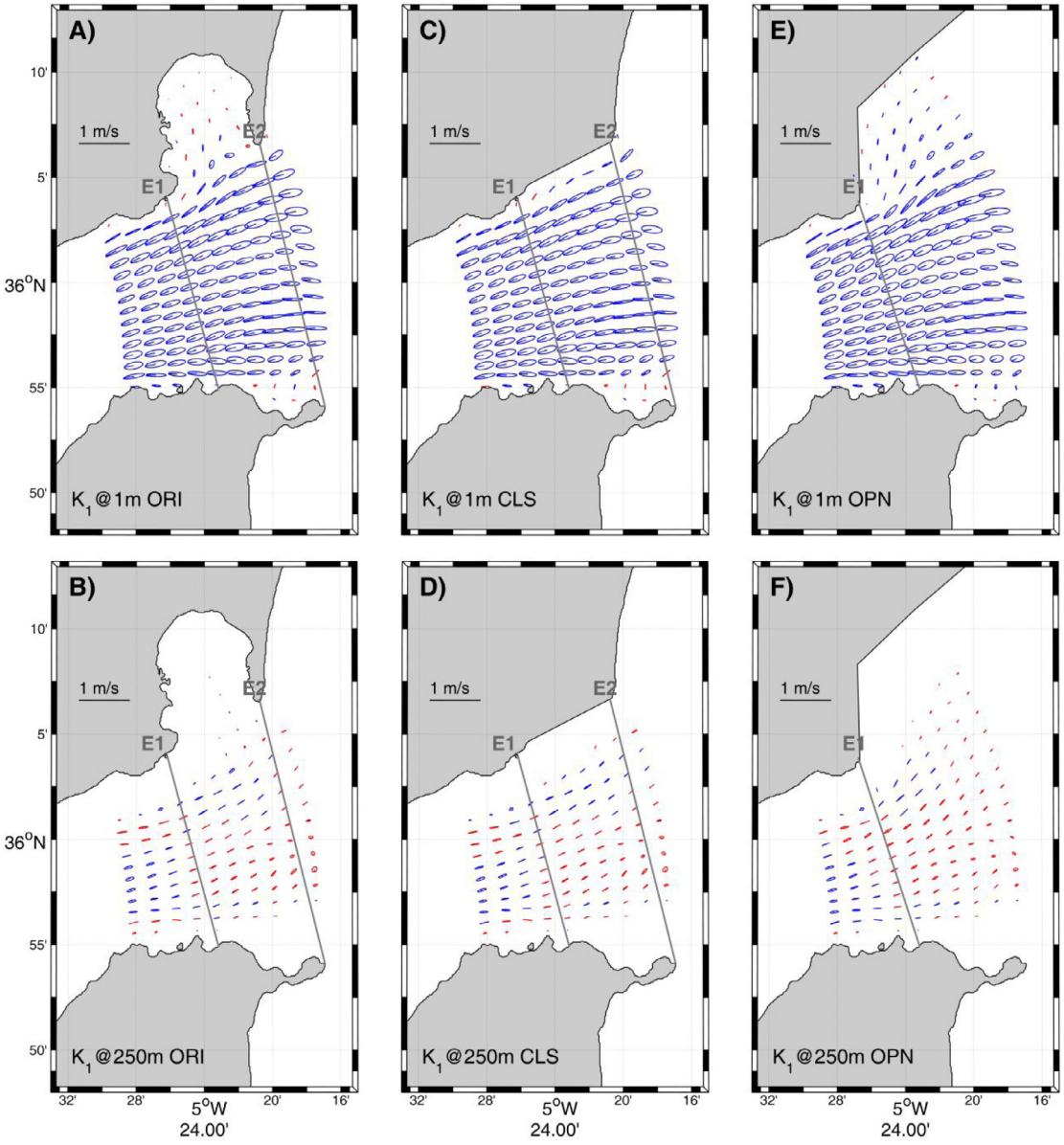

Fig. 10. Same as Fig. 9 except for K_1 constituent . (For interpretation of the references to color in this figure legend, the reader is referred to the web version of this article.)

Average properties of the exchange such as the mean exchanged flows or the location and salinity that characterize the mean interface remain unaltered except for very small changes that take place nearby the Algeciras Bay. The only possible exception is provided by the OPN configuration, which gives a very slight increase of the exchanged flows (Fig. 6A). This increase is compatible with the shorter Strait featured by the OPN configuration, as short straits are less topographically-constraining (Helfrich, 1995). It is also compatible with the minimum salinity of the inflow of all configurations (Table 1, Section 4.3) or, alternately, with the maximum inflow–outflow salinity contrast (hence, density contrast), which is the driving force of hydraulically controlled two-layer flows, such as the case of the exchange through the Strait of Gibraltar (Armi and Farmer, 1985, 1988).

At local scale, however, obvious differences which mainly affect the semidiurnal tide are found between the three configurations in the vicinity of the Bay of Algeciras. Fig. 5A and B (also 9A and B) show a noticeable penetration of M_2 into the Bay in the ORI configuration and indicates that it is a small buffer for semidiurnal flows. In fact, this configuration gives M_2 signals of 0.055 $\pm$ 0.005 Sv and 0.053 $\pm$ 0.005 Sv amplitude across the southern boundary section AB (Fig. 1) for the Atlantic and Mediterranean layers, respectively (the small difference is necessary in order to account for the vertical tide), which agrees with Sammartino et al. (2014). They are non-negligible fractions of the Atlantic layer M_2 transport in the eastern part of the Strait, especially across section E2 (Table 2). Notice that this is a specific feature of semidiurnal tide since diurnal constituents hardly penetrate into the Bay (Fig. 5C and D).

This role as a buffer has important biological consequences, as mentioned in the Introduction (Fig. 2), because the residence time of parcels of nutrient-enriched surface water in the Bay is noticeably increased with regards to the transit time in the Strait of similar water parcels advected by the Atlantic Jet (0.5–1 day for an averaged surface layer speed of 0.5–1 m s^{-1} against $\sim$4 days of residence within the Bay). Available energy for mixing at semidiurnal (mainly M_2) frequencies is an important ingredient of the enrichment process that allows the Bay to sustain high

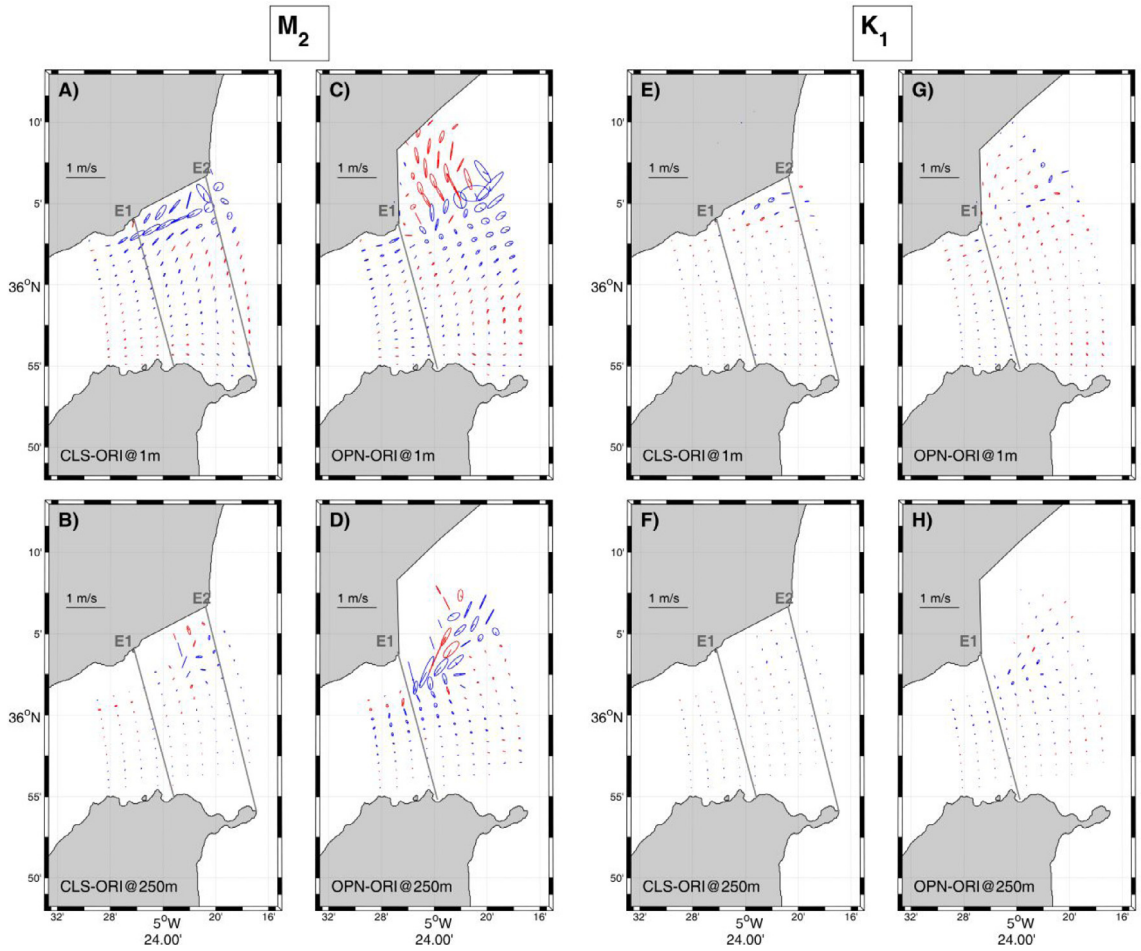

Fig. 11. Residual M_2 (four panels on the left) and K_1 (four panels on the right) tidal ellipses produced by the harmonic analysis applied on the series obtained by subtracting ORI output from CLS output (panels (A) and (B) for M_2; panels (E) and (F) for K1), and by subtracting ORI output from OPN output (panels (C) ad (D) for M_2; panels (G) and (H) for K_1). Top row is for surface (1 m depth), and bottom row is for 250 m depth. Velocity scale is the same in all panels for comparison purposes. Sections E1 and E2 have been indicated.

levels of primary production and turn it into a much more productive area than the Strait itself. Obviously this buffer does not exist in the OPN and CLS configurations, an absence which would have consequences for the productivity of the neighbor Alborán basin. Therefore, even though the dynamical effects of the Bay on the global properties of the exchange through the Strait are of little importance, its impact as fertilizer of the Alboran Sea (and Mediterranean Sea to a lesser extend) would not be so irrelevant.

Acknowledgments

Financial support from the Spanish Economy and Competitiveness Ministry through the Research Project ENCIBA (CTM2013-40886-P) and from the Regional Government Junta de Andalucía through the Excellence Research Project MOCBASE (P12-RNM-1540) are acknowledged. Model simulations have been run in the Supercomputing and Bioinnovation Center of the University of Málaga (PICASSO). C.N. acknowledges the postdoctoral fellowship from the University of Málaga.

References

Álvarez Fanjul, E., Pérez Gómez, B., Rodríguez Sánchez Arévalo, I., 2001. Nivmar: a storm surge forecasting system for Spanish waters. Sci. Mar. 65 (S1), 145–154.

Armi, L., Farmer, D.M., 1985. The internal hydraulics of the strait of gibraltar and associated sills and narrows. Oceanol. Acta 8, 37–46.

Armi, L., Farmer, D.M., 1988. The flow of Mediterranean water through the Strait of Gibraltar. Prog. Oceanogr. 21 (1), 1–103. http://dx.doi.org/10.1016/0079-6611(88)90055-9.

Bryden, H.L., Candela, J., Kinder, T.H., 1994. Exchange through the Strait of Gibraltar. Prog. Oceanogr. 33 (3), 201–248. http://dx.doi.org/10.1016/0079-6611(94)90028-0.

Candela, J., Winant, C.D., Bryden, H.L., 1989. Meteorologically forced subinertial flows through the Strait of Gibraltar. J. Geophys. Res. 94 (C9), 12667. http://dx.doi.org/10.1029/JC094iC09p12667.

Candela, J., Winant, C., Ruiz, A., 1990. Tides in the Strait of Gibraltar. J. Geophys. Res.: Oceans 95 (C5), 7313–7335. http://dx.doi.org/10.1029/JC095iC05p07313.

Carrère, L., Lyard, F., 2003. Modeling the barotropic response of the global ocean to atmospheric wind and pressure forcing - comparisons with observations. Geophys. Res. Lett. 30 (6), 1275. http://dx.doi.org/10.1029/2002GL016473.

Cats, G., Wolters, L., 1996. The Hirlam project [meteorology]. IEEE Comput. Sci. Eng. 3, 4–7. http://dx.doi.org/10.1109/99.556505.

Chioua, J., Dastis, C., González, C.J., Reyes, E., Mañanes, R., Ruiz, M.I., … Bruno, M., 2017. Water exchange between algeciras bay and the strait of gibraltar: A study based on HF coastal radar. Estuar. Coast. Shelf Sci. 196, 109–122. http://dx.doi.org/10.1016/j.ecss.2017.06.030.

Defant, A., 1961. Physical Oceanography. Pergamon Press, New York.

Farmer, D.M., Armi, L., 1988. The flow of Atlantic water through the Strait of Gibraltar. Prog. Oceanogr. 21 (1), 1–103. http://dx.doi.org/10.1016/0079-6611(88)90055-9.

García Lafuente, J., Almazán, J.L., Castillejo, F., Khribeche, A., Hakimi, A., 1990. Sea level in the strait of gibraltar: Tides. Int. Hydrographic Rev. 47, 111–130.

García Lafuente, J., Álvarez Fanjul, E., Vargas, J.M., Ratsimandresy, A.W., 2002. Subinertial variability in the flow through the Strait of Gibraltar. J. Geophys. Res.: Oceans 107 (C10), 3168. http://dx.doi.org/10.1029/2001JC001104.

García Lafuente, J., Bruque Pozas, E., Sánchez Garrido, J.C., Sannino, G., Sammartino, S., 2013. The interface mixing layer and the tidal dynamics at

the eastern part of the Strait of Gibraltar. J. Mar. Syst. 117–118, 31–42. http://dx.doi.org/10.1016/j.jmarsys.2013.02.014.

García Lafuente, J., Naranjo, C., Sammartino, S., Sánchez-Garrido, J.C., Delgado, J., 2017. The Mediterranean outflow in the Strait of Gibraltar and its connection with upstream conditions in the Alborán Sea. Ocean Science 13 (2), 195–207.

García Lafuente, J., Sarhan, T., Vargas, M., Vargas, J.M., Plaza, F., 1999. Tidal motions and tidally induced fluxes through la Línea submarine canyon, western Alboran Sea. J. Geophys. Res.: Oceans 104 (C2), 3109–3119. http://dx.doi.org/10.1029/1998JC900039.

García Lafuente, J., Vargas, J.M., Plaza, F., Sarhan, T., Candela, J., Bascheck, B., . Bascheck, B., 2000. Tide at the eastern section of the Strait of Gibraltar. J. Geophys. Res.: Oceans 105 (C6), 14197–14213. http://dx.doi.org/10.1029/2000JC900007.

Helfrich, K.R., 1995. Time-dependent two-layer hydraulic exchange flows. J. Phys. Oceanogr. 25 (3), 359–373. http://dx.doi.org/10.1175/1520-0485(1995)025{<}0359:TDTLHE{>}2.0.CO;2.

Marshall, J., Adcroft, A., Hill, C., Perelman, L., Heisey, C., 1997. A finite-volume, incompressible Navier Stokes model for studies of the ocean on parallel computers. J. Geophys. Res.: Oceans 102 (C3), 5753–5766. http://dx.doi.org/10.1029/96JC02775.

Naranjo, C., Garcia-Lafuente, J., Sannino, G., Sanchez-Garrido, J.C., 2014. How much do tides affect the circulation of the Mediterranean Sea? From local processes in the Strait of Gibraltar to basin-scale effects. Prog. Oceanogr. 127, 108–116. http://dx.doi.org/10.1016/j.pocean.2014.06.005.

Navascues, B., et al., 2013. Long-term varification of HIRLAM and ECMWF forecasts over Southern Europe: History and perspectives of Numerical Weather Prediction at AEMET. Atmos. Res. 125–126, 20–33. http://dx.doi.org/10.1016/j.atmosres.2013.01.010.

Pawlowicz, R., Beardsley, B., Lentz, S., 2002. Classical tidal harmonic analysis including error estimates in MATLAB using T_TIDE. Comput. Geosci. 28 (8), 929–937. http://dx.doi.org/10.1016/S0098-3004(02)00013-4.

Peliz, A., Boutov, D., Cardoso, R.M., Delgado, J., Soares, P.M.M., 2013. The gulf of Cadiz–alboran sea sub-basin: Model setup, exchange and seasonal variability. Ocean Modell. 61, 49–67. http://dx.doi.org/10.1016/j.ocemod.2012.10.007.

Periáñez, R., 2012. Modelling the environmental behaviour of pollutants in Algeciras Bay (south Spain). Mar. Pollut. Bull. 64 (2), 221–232. http://dx.doi.org/10.1016/j.marpolbul.2011.11.030.

Sammartino, S., García Lafuente, J., Naranjo, C., Sánchez Garrido, J.C., Sánchez Leal, R., Sánchez Román, A., 2015. Ten years of marine current measurements in espartel sill, strait of gibraltar. J. Geophys. Res. C 120 (9), 6309–6328. http://dx.doi.org/10.1002/2014JC010674.

Sammartino, S., García Lafuente, J., Sánchez Garrido, J.C., De los Santos, F.J., Álvarez Fanjul, E., Naranjo, C., . Calero, C., 2014. A numerical model analysis of the tidal flows in the Bay of Algeciras, Strait of Gibraltar. Cont. Shelf Res. 72, 34–46. http://dx.doi.org/10.1016/j.csr.2013.11.002.

Sammartino, S., Sánchez-Garrido, J.C., Naranjo, C., García Lafuente, J., Rodríguez Rubio, P., Sotillo, M., 2018. Water renewal in semi-enclosed basins: A high resolution Lagrangian approach with application to the Bay of Algeciras, Strait of Gibraltar. Limnol. Oceanogr.: Methods 16 (2), 106–118. http://dx.doi.org/10.1002/lom3.10231.

Sánchez Garrido, J.C., García Lafuente, J., Criado Aldeanueva, F., Baquerizo, A., Sannino, G., 2008. Time-spatial variability observed in velocity of propagation of the internal bore in the Strait of Gibraltar. J. Geophys. Res. 113 (C7), C07034. http://dx.doi.org/10.1029/2007JC004624.

Sánchez Garrido, J.C., García Lafuente, J., Álvarez Fanjul, E., Sotillo, M.G., de los Santos, F.J., 2013. What does cause the collapse of the Western Alboran Gyre? Results of an operational ocean model. Prog. Oceanogr. 116, 142–153. http://dx.doi.org/10.1016/j.pocean.2013.07.002.

Sánchez Garrido, J.C., García Lafuente, J., Sammartino, S., Naranjo, C., de los Santos, F.J., Álvarez Fanjul, E., 2014. Meteorologically-driven circulation and flushing times of the Bay of Algeciras, Strait of Gibraltar. Mar. Pollut. Bull. 80, 97–106, Retrieved from http://www.sciencedirect.com/science/article/pii/S0025326X1400037X.

Sánchez Garrido, J.C., Sannino, G., Liberti, L., García-afuente, J., Pratt, L., 2011. Numerical modeling of three-dimensional stratified tidal flow over Camarinal Sill, Strait of Gibraltar. J. Geophys. Res.: Oceans 116 (C12), C12026. http://dx.doi.org/10.1029/2011JC007093.

Sánchez Román, A., García Lafuente, J., Delgado, J., Sánchez Garrido, J.C., Naranjo, C., 2012. Spatial and temporal variability of tidal flow in the Strait of Gibraltar. J. Mar. Syst. 98–99, 9–17. http://dx.doi.org/10.1016/j.jmarsys.2012.02.011.

Sannino, G., Bargagli, A., Artale, V., 2004. Numerical modeling of the semidiurnal tidal exchange through the Strait of Gibraltar. J. Geophys. Res.: Oceans 109 (C5), C05011. http://dx.doi.org/10.1029/2003JC002057.

Sannino, G., Carillo, A., Pisacane, G., Naranjo, C., 2015. On the relevance of tidal forcing in modelling the Mediterranean thermohaline circulation. Prog. Oceanogr. http://dx.doi.org/10.1016/j.pocean.2015.03.002.

Sotillo, M.G., Cailleau, S., Lorente, P., Levier, B., Aznar, R., Reffray, G., . Alvarez-Fanjul, E., 2015. The myocean IBI ocean forecast and reanalysis systems: operational products and roadmap to the future copernicus service. J. Operat. Oceanogr. 8 (1), 63–79. http://dx.doi.org/10.1080/1755876X.2015.1014663.

Soto-Navarro, J., Lorente, P., Álvarez Fanjul, E., Carlos Sánchez-Garrido, J., García-Lafuente, J., 2016. Surface circulation at the strait of gibraltar: A combined HF radar and high resolution model study. J. Geophys. Res.: Oceans 121 (3), 2016–2034. http://dx.doi.org/10.1002/2015JC011354.

Volpe, G., Colella, S., Forneris, V., Tronconi, C., Santoleri, R., 2012. The mediterranean ocean colour observing system & amp; ndash; system development and product validation. Ocean Sci. 8 (5), 869–883. http://dx.doi.org/10.5194/os-8-869-2012.

Wang, D.-P., 1989. Model of mean and tidal flows in the Strait of Gibraltar. Deep Sea Res. A 36 (10), 1535–1548. http://dx.doi.org/10.1016/0198-0149(89)90056-3, JOUR..